Dalton Transactions

ROYAL SOCIETY OF CHEMISTRY

PAPER

View Article Online
View Journal

Cite this: DOI: 10.1039/d0dt03277h

Magnetic structure and uniaxial negative thermal expansion in antiferromagnetic CrSb

Jibao Yuan,[a] Yuzhu Song, *[a] Xianran Xing [b] and Jun Chen [a]

Received 20th September 2020,
Accepted 17th November 2020

DOI: 10.1039/d0dt03277h

rsc.li/dalton

Negative thermal expansion (NTE) has been found in a growing number of ferromagnetic and ferrimagnetic materials; however, it remains a challenge to discover antiferromagnetic (AFM) NTE materials. Here, we report the uniaxial NTE properties of AFM intermetallic CrSb systematically, and reveal its uniaxial NTE mechanism for the first time. The present AFM intermetallic CrSb shows uniaxial NTE at high temperature and over a broad temperature window (α_a = −6.55 × 10^{-6} K^{-1}, 360–600 K). The direct experimental evidence of neutron powder diffraction reveals that NTE is induced by the AFM ordering of the Cr atom. The present study demonstrates that due to the transition from an AFM ordered structure to a paramagnetic disordered configuration, the negative contribution to the thermal expansion from the magnetovolume effect overwhelms the positive contribution from anharmonic phonon vibration. This study is of interest to find antiferromagnetic NTE materials.

Introduction

Negative thermal expansion (NTE), in which at least one of all the three dimensions of the material decreases with increasing temperature, is an unusual and unexpected thermodynamic phenomenon.[1–3] Due to their ability to compensate for the normal positive thermal expansion (PTE) and great potential for technological and industrial applications in high-precision instruments and some important transportation facilities, NTE materials have attracted a tremendous upsurge of interest.[2,4] Since the isotropic NTE of ZrW_2O_8 was studied in 1996,[1] the research on NTE has developed rapidly in the past two decades.[5,6] Meanwhile, multifarious NTE materials have been found, such as oxides,[7,8] alloys,[9–11] anti-perovskite manganese nitrides,[12–14] fluorides,[15,16] $PbTiO_3$-based ferroelectrics,[17] cyanides[18,19] and metal–organic frameworks (MOFs).[20] These studies shed light on the underlying microscopic NTE mechanism such as low-frequency phonon transverse vibration,[21] valence transition,[22,23] magnetovolume effect,[24] ferroelectricity[25] and microstructural effects.[26] However, most of the NTE materials that have been found are ceramic materials, and the quantity of NTE alloys or intermetallic compounds is still limited. It is known that metallic materials have a broader prospect in modern applications because of their superior mechanical performance as well as remarkable thermal and electrical conductivity. Therefore, there is an urgent need to discover novel NTE metallic materials for further applications.

The most representative research on NTE alloys is the abnormal thermal expansion of magnetic Invar alloys ($Fe_{65}Ni_{35}$) discovered by the Swiss physicist C. É. Guillaume in 1897,[27] who was awarded the Nobel Prize in Physics.[28] The theory of the magnetovolume effect (MVE) caused by the variation of the amplitude of the local magnetic moment can account for the anomalous phenomenon of Invar alloys.[29] In general, the volume of magnetic materials with an ordered magnetic configuration is larger than that of magnetic materials with a disordered magnetic structure,[30] which means that the MVE has a negative contribution to the thermal expansion. Undoubtedly, the overall thermal expansion hinges on the balance between the MVE and anharmonic phonons, in which the phonons contribute to PTE. Hence, if the negative contribution of the MVE can outweigh the positive contribution of the phonons, total NTE will occur. Moreover, on the basis of the MVE theory, ground-breaking progress has been made in the research of magnetic NTE metal-based compounds, such as Invar alloys,[27,28,31] (Hf,Nb)Fe_2,[32] $NaZn_{13}$-type compounds,[9,33] R_2Fe_{17},[34] (Sc,Ti)Fe_2[35] and (Zr,Nb)Fe_2.[36] It should be noted that these NTE metal-based compounds are ferromagnetic or ferrimagnetic. However, the discovery of antiferromagnetic NTE metal-based materials remains challenging. More recently, NTE has been observed in some antiferromagnetic functional materials, such as the Mn_3XN antiferromagnet with many fascinating physical phenomena,[12,37–45] the noncollinear antiferromagnet Mn_3Ge with a large anomalous Hall effect[46] and the well-known CrAs-based superconductivity

[a]Beijing Advanced Innovation Centre for Materials Genome Engineering, Department of Physical Chemistry and School of Mathematics and Physics, University of Science and Technology Beijing, Beijing 100083, China. E-mail: yuzhusong@xs.ustb.edu.cn
[b]Beijing Advanced Innovation Centre for Materials Genome Engineering and Institute of Solid State Chemistry, University of Science and Technology Beijing, Beijing 100083, China

compounds.[47] It is well known that the dimensions of antiferromagnetic materials are quite insensitive to the external magnetic field because they have no macroscopic net magnetization.[48] Therefore, the discovery of antiferromagnetic NTE compounds will enable crucial theoretical and practical applications of significance.

The antiferromagnetic compound CrSb has a simple hexagonal nickel arsenide structure and exhibits magnetic ordering at room temperature.[49,50] It is noteworthy that in 1953, A. I. Snow first investigated the thermal expansion properties of antiferromagnetic CrSb.[51] Intriguingly, the linear coefficient of thermal expansion (CTE) of CrSb along the *a*-axis was observed to be negative by the X-ray diffraction technique. However, this counterintuitive phenomenon has not yet been explained. Uniaxial NTE widely exists in organic crystalline materials,[52] metallic materials,[53,54] symmetry-broken layered perovskites[55] and other systems.[56,57] In view of the advantages of antiferromagnetic NTE materials, herein the abnormal thermal expansion behavior of antiferromagnetic CrSb was studied by variable temperature neutron powder diffraction (NPD).

In this work, we study the thermal expansion in the antiferromagnetic intermetallic compound CrSb, which exhibits uniaxial NTE ($\alpha_a = -6.55 \times 10^{-6}$ K^{-1}, 360–600 K) at elevated temperatures and in a wide temperature range. The crystal and magnetic structures of CrSb intermetallics have been determined by the Rietveld method from NPD data at temperatures 5–600 K. Its uniaxial NTE is induced by the antiferromagnetic ordering controlled by the Cr magnetic moment. It should be noted that it is the first time that the uniaxial NTE mechanism of the antiferromagnetic compound CrSb is revealed. The experimental evidence indicates that the anisotropic NTE behavior and MVE are inextricably linked, which will promote the discovery of NTE in other magnetic functional materials.

Experimental

A polycrystalline CrSb intermetallic sample was prepared by direct solid-state reaction using Cr (99.99%) and Sb (99.99%) powders as raw materials. Firstly, the stoichiometric powders were weighed and ground in an agate mortar for about 1 hour to ensure that they were well mixed and then the mixed powders were pressed into a pellet with a tablet press. After that, the pellet was heated slowly to 645 °C in a vacuum-sealed quartz tube, held at this temperature for 2 hours, and then annealed at a temperature between 645 °C and 900 °C for 36 hours.[58] The annealing temperatures were chosen so that the samples do not melt. The samples were reground and annealing was repeated.[59] Finally, the sample was cooled naturally to room temperature in the furnace. The temperature dependence of NPD data with $\lambda = 2.41$ Å was collected using a Wombat high-intensity diffractometer of the Australian Nuclear Science and Technology Organisation (ANSTO). The crystal and magnetic structure refinements for all NPD data were analysed using the FULLPROF software. The macroscopic magnetic properties were measured using a Quantum Design physical property measurement system (PPMS) with a vibrating sample magnetometer (VSM).

Results and discussion

As illustrated in Fig. 1a, CrSb exhibits highly anisotropic thermal expansion properties. For example, the CTEs of different crystal axes above 360 K are a mix of negative and positive values. The linear CTE of CrSb along the *a*-axis is $\alpha_a = -6.55 \times 10^{-6}$ K^{-1} (360–600 K), which is similar to that of some antiferromagnetic anti-perovskites. For example, the CTE of $Mn_3(Ga_{0.5}Ge_{0.4}Mn_{0.1})N$ is around -3×10^{-6} K^{-1} above 334 K.[12] Besides, the CTE of $Mn_3Ga_{0.3}Sn_{0.7}N$ is -8.1×10^{-6} K^{-1} in the temperature range of 418–454 K.[39] It should be noted that due to the limitations of experimental conditions, the temperature of the thermal expansion property analysis can only be measured to 600 K, but at even higher temperature (below the Néel temperature), the CTE along the *a*-axis of CrSb should be still negative. However, a strong PTE is found along the *c*-axis over the whole temperature range, and the CTE is as high as $\alpha_c = 56.97 \times 10^{-6}$ K^{-1} (360–600 K), which is about one order of magnitude higher than the absolute value of α_a, agreeing with

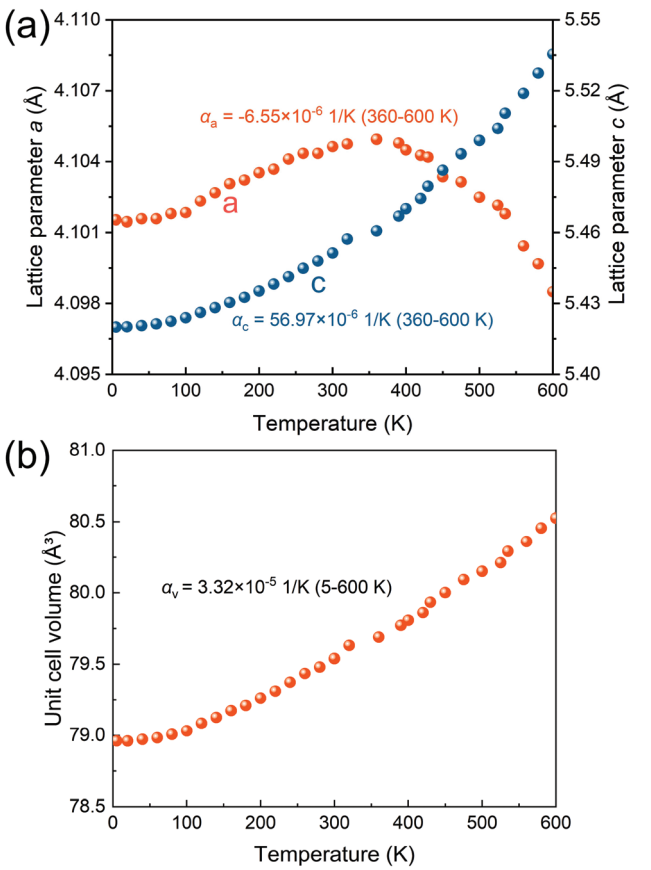

Fig. 1 Temperature dependence of (a) the lattice parameters and (b) unit cell volume of the CrSb intermetallic compound.

the previous literature results.[51] As a result, the whole unit cell of CrSb presents a large PTE determined as $\alpha_V = 3.32 \times 10^{-5}$ K^{-1} (5–600 K) (Fig. 1b). Obviously, the uniaxial NTE appears in the high temperature region and is maintained over a wide range of temperatures, which is quite uncommon among the numerous NTE materials families that have been discovered. For example, the anisotropic NTE along the *a* direction when it is below about 150 K was observed in the bulk CuO which was attributed to the preferable enhancement of the superexchange interaction along [10 $\bar{1}$].[60] In addition, abnormal NTE occurs in the *c*-axis of Cr_2GaN when the temperature is lower than 170 K.[54] It should be noted that the dimensions of the ferromagnetic compounds change with the external magnetic field, while those of the antiferromagnets are not affected. More importantly, in recent years, a large number of studies have shown that antiferromagnetic materials are outstanding candidates in the context of spintronic applications.[61] Similarly, antiferromagnetic NTE materials are expected to be applied in the field of spintronics due to their anti-interference to a magnetic field.

In order to reveal the reason for the shrinkage of the *a*-axis in CrSb intermetallics, the crystal structure extracted from the variable temperature NPD data was analysed in depth. As indicated in Fig. 2a, CrSb has a hexagonal crystal structure of NiAs type (space group: *P*63/*mmc*), in which Cr and Sb atoms occupy the Wyckoff sites of 2*a* (0, 0, 0) and 2*c* (1/3, 2/3, 1/4), respectively. The reason for *a*-axis contraction and *c*-axis expansion can be intuitively given as the temperature dependence of bond lengths and angles. The crystal structure from the perspective of the *bc* plane of CrSb is shown in Fig. 2b. The Cr and Sb atoms are connected and interacted by the Cr–Sb bond to form two bond angles, Sb–Cr–Sb and Cr–Sb–Cr angles. It is noteworthy that the distance between the nearest neighbour Cr atoms is half of the lattice parameter *c*,[49] which is governed by the fact that the Cr atoms occupy the midpoint of the *c* axis

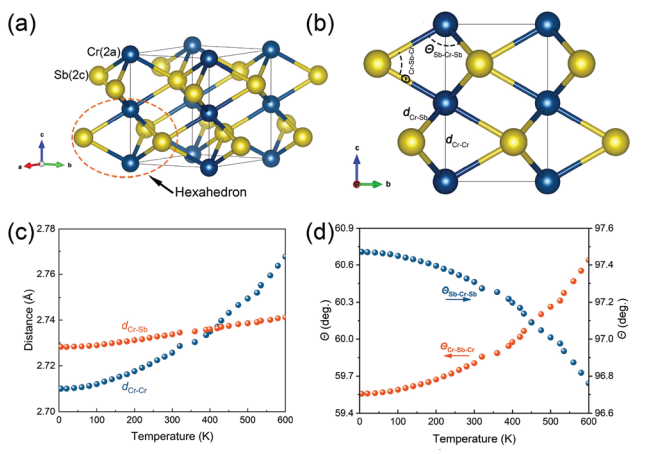

Fig. 2 (a) The hexagonal structure of CrSb (space group, *P*63/*mmc*). (b) Crystal structure in the *bc* plane of CrSb. Temperature dependence of (c) the bond distance of Cr–Sb and Cr–Cr and (d) bond angles including Sb–Cr–Sb and Cr–Sb–Cr.

in the unit cell of CrSb. The temperature dependence of the adjacent Cr–Sb distance and the nearest Cr–Cr distance obtained from the NPD data analysis are shown in Fig. 2c. It is incredible that both the Cr–Sb distance and the nearest Cr–Cr distance increase with increasing temperature in the whole temperature range. Additionally, it can also be seen obviously that the distance of the closest Cr–Cr atoms increases more rapidly than that of the Cr–Sb atoms. As a consequence, a large PTE can be found along the *c*-axis. On the other hand, it is not difficult to understand the cause of NTE along the *a*-axis by analysing the change of the bond angle with temperature. Combined with the crystal structure shown in Fig. 2a and b, the Cr–Cr distance along the *c*-axis expands with increasing temperature, so the chemical bond angle of Cr–Sb–Cr increases and that of Sb–Cr–Sb decreases (Fig. 2d), which indirectly leads to the Sb atoms in the *ab* plane coming closer and closer. In other words, the NTE of the *a*-axis originates from the shrinkage of the Cr_2Sb_3 hexahedron in the *ab* plane. Meanwhile, the elongation of the Cr_2Sb_3 hexahedron along the *c*-axis induces the PTE of the *c*-axis.

The above studies on the NTE mechanism of CrSb are carried out from the perspective of the crystal structure, but what is the essential reason for such an abnormal thermal expansion behavior? Due to the MVE, the NTE phenomena of most magnetic materials are related to magnetic ordering.[2,62,63] For example, the giant NTE in anti-perovskite manganese nitrides is associated with the gradual increase of the Γ^{5g} antiferromagnetic ordering moment.[12,37–45] Therefore, the magnetic structure information was extracted by carefully processing the variable temperature NPD data. The temperature dependence of NPD patterns for CrSb in the range of 30–120° and 5–600 K are plotted in Fig. 3a. The (100) and (002) peaks are marked particularly in Fig. 3a. It can be roughly seen that with the increase of temperature (above 360 K), the diffraction peak of (100) slightly shifts to the higher diffraction angle, while that of (002) gradually moves to the lower diffraction angle, which directly reflects the anisotropic thermal expansion characteristics of CrSb. In order to clarify the details of the evolution of the magnetic structure, the variation of magnetic peak intensity with temperature was studied. Obviously, as the temperature increases, the intensity of (002) almost remains unchanged, but that of (100) decreases gradually, especially around 360 K (Fig. 3b). This directly means that the direction of the magnetic moment in the magnetic structure is parallel to the *c* axis, which is basically in accordance with the past research studies.[49,59] Moreover, the decrease of the intensity of the (100) magnetic peak is caused by the transition from magnetic order to disorder. It can be observed that when the intensity of (100) decreases obviously at 360 K, the NTE behavior begins to appear, which directly indicates that the NTE phenomenon is profoundly complicated with the magnetic behavior.

The magnetic structure refinements of the NPD patterns of CrSb are shown in Fig. 4a. The previously conjectured magnetic structure model can fit the experimental data well, which suggests that the magnetic structure is antiferromagnetic. As

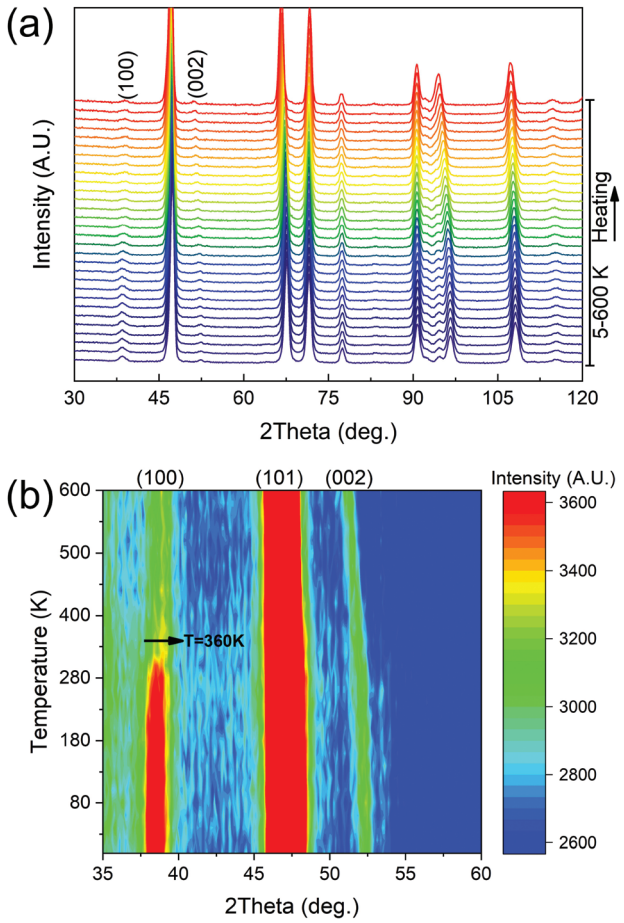

Fig. 3 (a) Temperature dependence of the neutron powder diffraction patterns of CrSb in the temperature range of 5–600 K. (b) Temperature dependence of the contour plots of the NPD profile intensity for the CrSb antiferromagnetic compound.

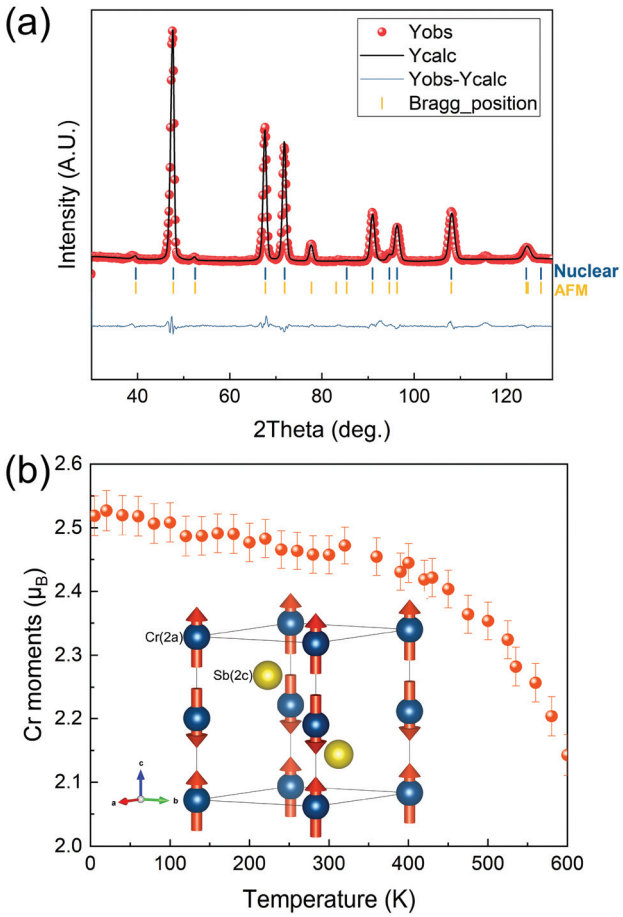

Fig. 4 (a) Magnetic structure refinements of the NPD patterns of CrSb at T = 300 K. (b) Temperature dependence of the magnetic moment of the Cr atom for the CrSb intermetallic compound. The inset shows the magnetic structure of CrSb intermetallics.

indicated in Fig. 4a, the refined NPD patterns contain two diffraction peaks of different signals, which come from nuclear scattering and magnetic scattering, respectively. The refined magnetic structure of CrSb is shown in Fig. 4b. It is antiferromagnetic below T_N and the Cr atoms located at the 2*a* site carry a moment which is coupled ferromagnetically within a given (001) layer and antiferromagnetically between successive layers, while the Sb atoms at the 2*c* site have no magnetic moment. In order to further verify the antiferromagnetic structure of CrSb, the macroscopic magnetic behavior of CrSb was studied. As shown in Fig. 5a, the macroscopic magnetization is very small and increases with the increase of temperature before the magnetic transition temperature. Unfortunately, due to the limitations of the measurement conditions, the temperature can only be measured to 400 K. Theoretically, if a higher temperature can be measured, the magnetization should increase first and then decrease, and a maximum inflection point will appear near the magnetic transition temperature. The *M*–*H* curve is almost linear and has no magnetic hysteresis (Fig. 5b). Moreover, the magnetization of *M*–*H* is relatively small, and it does not reach saturation even at H = 5 T, which is exactly the characteristic of antiferromagnetism. Based on the analysis of the *M*–*T* curve and *M*–*H* curve, it can be concluded that CrSb is antiferromagnetic, which is consistent with the antiferromagnetic structure obtained by NPD refinement. The temperature dependence of Cr magnetic moment is depicted in Fig. 4b. With increasing temperature, the magnetic moment of the Cr atom decreases nonlinearly from approximately 2.5μ_B to about 2.15μ_B. Since the temperature can only be measured to 600 K, it had not dropped to zero. However, it has no influence on revealing the uniaxial NTE mechanism of CrSb.

To further elucidate the correlation between magnetism and anomalous thermal expansion, the variation trend of the lattice parameter *a* and magnetic moment of the Cr atom with temperature are plotted in Fig. 6. It can be obviously seen that the thermal expansion can be divided into two independent regions. Taking 360 K as the boundary temperature, PTE is displayed below this temperature and NTE is displayed when it is higher than this temperature. When the magnetic moment of Cr decreases very slowly, almost unchanged below 360 K, the lattice parameter *a* expands, *i.e.*, PTE occurs; however, when

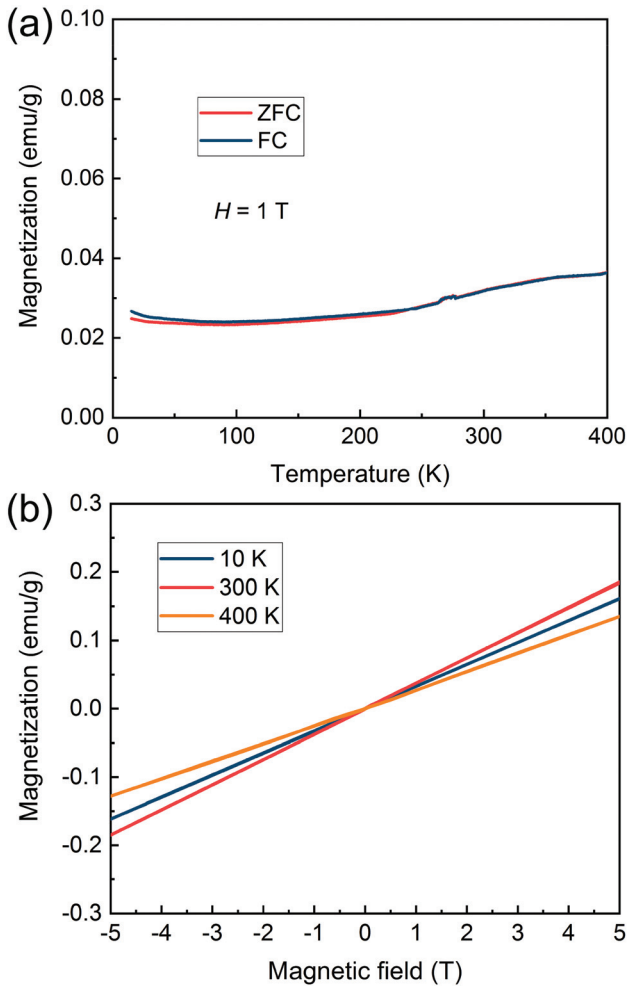

Fig. 5 (a) Temperature dependence of zero-field-cooling (ZFC) and field-cooling (FC) magnetization (M) at a magnetic field of H = 1 T for CrSb intermetallics. (b) The magnetic hysteresis loops (M–H) at selected temperatures for CrSb intermetallics.

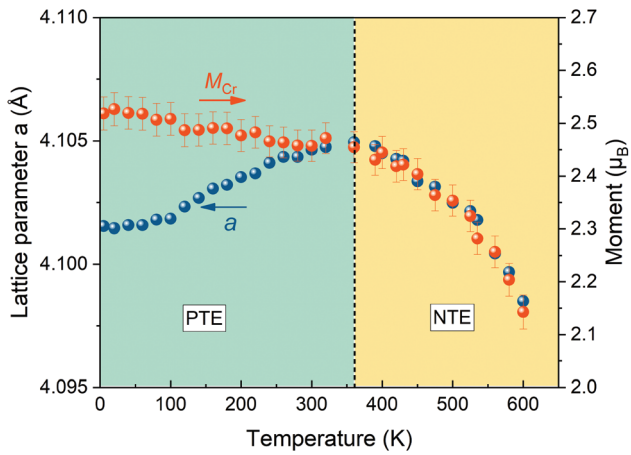

Fig. 6 Temperature dependence of the lattice parameter of a and magnetic moment of the Cr atom for the CrSb intermetallic compound.

the magnetic moment drops sharply (360–600 K), a begins to shrink, *i.e.*, NTE occurs. Moreover, it is interesting to note that the variation curves of the lattice parameter a and magnetic moment of the Cr atom nearly overlap and show a nonlinear decreasing trend. According to the MVE theory,[64] the volume of magnetic materials with an ordered magnetic configuration is larger than that of magnetic materials with a disordered magnetic structure, which means that the contribution of magnetic order to thermal expansion is negative.[65] Because the magnetic moment of Cr decreases very slowly below 360 K and MVE is relatively weak, the positive contribution to thermal expansion from anharmonic phonon vibration exceeds the spontaneous magnetostriction. In the temperature range of 360–600 K, the magnetic moment decreases rapidly, which indicates a stronger transition from antiferromagnetic order to paramagnetic disorder. As a result, the negative contribution of the spontaneous magnetostriction from antiferromagnetic ordering to thermal expansion overwhelms the positive contribution from anharmonic phonon vibration. Therefore, the contraction of the lattice parameter a can be attributed to the significant reduction of the Cr magnetic moment. Since the Cr atom has a magnetic moment but Sb does not, the nearest neighbour Cr atoms dominate the antiferromagnetic exchange interaction of CrSb. Therefore, the shrinkage in the ab plane and the elongation along the c-axis of the Cr_2Sb_3 hexahedron are controlled by the distance between the nearest Cr–Cr atoms. It should be noted that the thermal expansion behavior controlled by the inherent magnetic moment should be the mutual origin of NTE in magnetic materials. The present abnormal thermal expansion phenomena controlled by the magnetic moment have been found in other magnetic materials systems as well, such as the classic anti-perovskite manganese nitrides Mn_3XN.[12,37–45]

Conclusions

In summary, the intrinsic mechanism of anisotropic NTE in CrSb is revealed for the first time. The uniaxial NTE property in the high temperature region and over a relatively broad temperature window has been found in the CrSb compound ($\alpha_a = -6.55 \times 10^{-6}$ K^{-1}, 360–600 K). The crystal structure and antiferromagnetic structure of CrSb are extracted by the Rietveld method from variable temperature NPD data. The direct experimental evidence of variable temperature NPD reveals that the contraction of the a-axis is controlled by the Cr magnetic moment. The sharp decrease of the Cr magnetic moment causes the expansion of the nearest-neighbour Cr–Cr distance, which results in the Cr_2Sb_3 hexahedron shrinking in the ab plane and elongating along the c-axis, so that the anisotropic NTE occurs. Furthermore, the dimension of CrSb compound is not affected by the external magnetic field due to its antiferromagnetic property, which makes it have a broader application prospect in the field of spintronics. The present study on the magnetic moment controlled NTE in

CrSb will prompt the discovery of NTE in other magnetic materials.

Conflicts of interest

There are no conflicts to declare.

Acknowledgements

This work was supported by the National Natural Science Foundation of China (grant no. 21825102, 21731001 and 21590793) and the Fundamental Research Funds for the Central Universities, China (FRF-TP-18-001C2). We thank Dr Chinwei Wang for his assistance in collecting the neutron powder diffraction data using the Wombat high-intensity diffractometer of the Australian Nuclear Science and Technology Organisation (ANSTO).

Notes and references

1 T. A. Mary, J. S. O. Evans, T. Vogt and A. W. Sleight, *Science*, 1996, **272**, 90–92.
2 J. Chen, L. Hu, J. Deng and X. Xing, *Chem. Soc. Rev.*, 2015, **44**, 3522–3567.
3 J. S. O. Evans, *J. Chem. Soc., Dalton Trans.*, 1999, 3317–3326.
4 K. Takenaka, *Sci. Technol. Adv. Mater.*, 2012, **13**, 013001.
5 J. P. Attfield, *Nature*, 2011, **480**, 465–466.
6 M. T. Dove and H. Fang, *Rep. Prog. Phys.*, 2016, **79**, 066503.
7 J. S. O. Evans, T. A. Mary, T. Vogt, M. A. Subramanian and A. W. Sleight, *Chem. Mater.*, 1996, **8**, 2809–2823.
8 N. Shi, A. Sanson, Q. Gao, Q. Sun, Y. Ren, Q. Huang, D. O. De Souza, X. Xing and J. Chen, *J. Am. Chem. Soc.*, 2020, **142**, 3088–3093.
9 R. Huang, Y. Liu, W. Fan, J. Tan, F. Xiao, L. Qian and L. Li, *J. Am. Chem. Soc.*, 2013, **135**, 11469–11472.
10 L. F. Li, P. Tong, Y. M. Zou, W. Tong, W. B. Jiang, Y. Jiang, X. K. Zhang, J. C. Lin, M. Wang, C. Yang, X. B. Zhu, W. H. Song and Y. P. Sun, *Acta Mater.*, 2018, **161**, 258–265.
11 L. Li, P. Tong, W. Tong, W. Jiang, Y. Ding, H. Lin, J. Lin, C. Yang, F. Zhu, X. Zhang, X. Zhu, W. Song and Y. Sun, *Inorg. Chem.*, 2019, **58**, 16818–16822.
12 K. Takenaka and H. Takagi, *Appl. Phys. Lett.*, 2005, **87**, 261902.
13 Y. Sun, C. Wang, Y. Wen, L. Chu, H. Pan, M. Nie and M. Tang, *J. Am. Ceram. Soc.*, 2010, **93**, 2178–2181.
14 P. Tong, D. Louca, G. King, A. Llobet, J. C. Lin and Y. P. Sun, *Appl. Phys. Lett.*, 2013, **102**, 041908.
15 B. K. Greve, K. L. Martin, P. L. Lee, P. J. Chupas, K. W. Chapman and A. P. Wilkinson, *J. Am. Chem. Soc.*, 2010, **132**, 15496–15498.
16 L. Hu, J. Chen, J. Xu, N. Wang, F. Han, Y. Ren, Z. Pan, Y. Rong, R. Huang, J. Deng, L. Li and X. Xing, *J. Am. Chem. Soc.*, 2016, **138**, 14530–14533.
17 J. Chen, X. Xing, C. Sun, P. Hu, R. Yu, X. Wang and H. Li, *J. Am. Chem. Soc.*, 2008, **130**, 1144–1145.
18 A. L. Goodwin, M. Calleja, M. J. Conterio, M. T. Dove, J. S. O. Evans, D. A. Keen, L. Peters and M. G. Tucker, *Science*, 2008, **319**, 794–797.
19 Q. Gao, J. Wang, A. Sanson, Q. Sun, E. Liang, X. Xing and J. Chen, *J. Am. Chem. Soc.*, 2020, **142**, 6935–6939.
20 Y. Wu, A. Kobayashi, G. J. Halder, V. K. Peterson, K. W. Chapman, N. Lock, P. D. Southon and C. J. Kepert, *Angew. Chem., Int. Ed.*, 2008, **47**, 8929–8932.
21 A. L. Goodwin and C. J. Kepert, *Phys. Rev. B: Condens. Matter Mater. Phys.*, 2005, **71**, 140301.
22 Y. W. Long, N. Hayashi, T. Saito, M. Azuma, S. Muranaka and Y. Shimakawa, *Nature*, 2009, **458**, 60–63.
23 M. Azuma, W. T. Chen, H. Seki, M. Czapski, S. Olga, K. Oka, M. Mizumaki, T. Watanuki, N. Ishimatsu, N. Kawamura, S. Ishiwata, M. G. Tucker, Y. Shimakawa and J. P. Attfield, *Nat. Commun.*, 2011, **2**, 347.
24 Y. Song, J. Chen, X. Liu, C. Wang, J. Zhang, H. Liu, H. Zhu, L. Hu, K. Lin, S. Zhang and X. Xing, *J. Am. Chem. Soc.*, 2018, **140**, 602–605.
25 J. Chen, K. Nittala, J. S. Forrester, J. L. Jones, J. Deng, R. Yu and X. Xing, *J. Am. Chem. Soc.*, 2011, **133**, 11114–11117.
26 K. Takenaka, Y. Okamoto, T. Shinoda, N. Katayama and Y. Sakai, *Nat. Commun.*, 2017, **8**, 14102.
27 C. É. Guillaume, *C. R. Acad. Sci.*, 1897, **125**, 18.
28 P. Mohn, *Nature*, 1999, **400**, 18–19.
29 M. Van Schilfgaarde, I. A. Abrikosov and B. Johansson, *Nature*, 1999, **400**, 46–49.
30 Y. Nakamura, *IEEE Trans. Magn.*, 1976, **12**, 278–291.
31 T. Yokoyama and K. Eguchi, *Phys. Rev. Lett.*, 2013, **110**, 075901.
32 Y. Song, J. Chen, X. Liu, C. Wang, Q. Gao, Q. Li, L. Hu, J. Zhang, S. Zhang and X. Xing, *Chem. Mater.*, 2017, **29**, 7078–7082.
33 Y. Song, R. Huang, Y. Liu, Z. Zhang, Q. Huang, Y. Jiang, S. Wang, L. Li, X. Xing and J. Chen, *Chem. Mater.*, 2020, **32**, 7535–7541.
34 D. Givord and R. Lemaire, *IEEE Trans. Magn.*, 1974, **10**, 109–113.
35 Y. Song, Q. Sun, M. Xu, J. Zhang, Y. Hao, Y. Qiao, S. Zhang, Q. Huang, X. Xing and J. Chen, *Mater. Horiz.*, 2020, **7**, 275–281.
36 Y. Song, Q. Sun, T. Yokoyama, H. Zhu, Q. Li, R. Huang, Y. Ren, Q. Huang, X. Xing and J. Chen, *J. Phys. Chem. Lett.*, 2020, **11**, 1954–1961.
37 C. Wang, L. Chu, Q. Yao, Y. Sun, M. Wu, L. Ding, J. Yan, Y. Na, W. Tang, G. Li, Q. Huang and J. W. Lynn, *Phys. Rev. B: Condens. Matter Mater. Phys.*, 2012, **85**, 220103.
38 Y. Sun, C. Wang, Q. Huang, Y. Guo, L. Chu, M. Arai and K. Yamaura, *Inorg. Chem.*, 2012, **51**, 7232–7236.
39 K. Shi, Y. Sun, C. V. Colin, L. Wang, J. Yan, S. Deng, H. Lu, W. Zhao, Y. Kazunari, P. Bordet and C. Wang, *Phys. Rev. B: Condens. Matter Mater. Phys.*, 2018, **97**, 054110.

40 S. Deng, Y. Sun, H. Wu, Q. Huang, J. Yan, K. Shi, M. I. Malik, H. Lu, L. Wang, R. Huang, L. Li and C. Wang, *Chem. Mater.*, 2015, **27**, 2495–2501.
41 J. C. Lin, P. Tong, W. Tong, Y. M. Zou, C. Yang, F. Zhu, X. K. Zhang, L. F. Li, M. Wang, Y. Wu, S. Lin, W. H. Song, X. B. Zhu and Y. P. Sun, *Scr. Mater.*, 2018, **152**, 6–10.
42 J. C. Lin, P. Tong, X. J. Zhou, H. Lin, Y. W. Ding, Y. X. Bai, L. Chen, X. G. Guo, C. Yang, B. Song, Y. Wu, S. Lin, W. H. Song and Y. P. Sun, *Appl. Phys. Lett.*, 2015, **107**, 131902.
43 X. G. Guo, P. Tong, J. C. Lin, C. Yang, K. Zhang, M. Wang, Y. Wu, S. Lin, W. H. Song and Y. P. Sun, *Scr. Mater.*, 2017, **128**, 74–77.
44 K. Takenaka, M. Ichigo, T. Hamada, A. Ozawa, T. Shibayama, T. Inagaki and K. Asano, *Sci. Technol. Adv. Mater.*, 2014, **15**, 015009.
45 K. Takenaka and H. Takagi, *Appl. Phys. Lett.*, 2009, **94**, 131904.
46 Y. Song, Y. Qiao, Q. Huang, C. Wang, X. Liu, Q. Li, J. Chen and X. Xing, *Chem. Mater.*, 2018, **30**, 6236–6241.
47 Y. Hu, X. Zheng, G. Ma, H. Lu, L. Zhang, C. Zhang, Y. Xia, Y. Hao, L. He, J. Chen, F. Shen, S. Wang, C. Wang, D. Wang and Y. Du, *Phys. Rev. Appl.*, 2019, **12**, 034027.
48 S. M. Rezende, A. Azevedo and R. L. Rodríguez-Suárez, *J. Appl. Phys.*, 2019, **126**, 151101.
49 A. I. Snow, *Phys. Rev.*, 1952, **85**, 365.
50 W. Reimers, E. Hellner, W. Treutmann, P. J. Brown and G. Heger, *J. Magn. Magn. Mater.*, 1980, **15–18**, 479–480.
51 A. I. Snow, *Rev. Mod. Phys.*, 1953, **25**, 127.
52 D. Das, T. Jacobs and L. J. Barbour, *Nat. Mater.*, 2010, **9**, 36–39.
53 Q. Lin and J. D. Corbett, *J. Am. Chem. Soc.*, 2012, **134**, 4877–4884.
54 H. Tong, S. Lin, Y. Huang, P. Tong, W. Song and Y. Sun, *Intermetallics*, 2019, **105**, 39–43.
55 C. Ablitt, S. Craddock, M. S. Senn, A. A. Mostofi and N. C. Bristowe, *npj Comput. Mater.*, 2017, **3**, 44.
56 Q. Li, H. Zhu, L. Zheng, L. Fan, Y. Ren, J. Chen, J. Deng and X. Xing, *Adv. Sci.*, 2016, **3**, 1600108.
57 V. V. Atuchin, F. Liang, S. Grazhdannikov, L. I. Isaenko, P. G. Krinitsin, M. S. Molokeev, I. P. Prosvirin, X. Jiang and Z. Lin, *RSC Adv.*, 2018, **8**, 9946–9955.
58 W. Reimers, E. Hellner, W. Treutmann and G. Heger, *J. Phys. C: Solid State Phys.*, 1982, **15**, 3597–3615.
59 W. J. Takei, D. E. Cox and G. Shirane, *Phys. Rev.*, 1963, **129**, 2008–2018.
60 Y. Zhang, M. McDonnell, S. A. Calder and M. G. Tucker, *J. Am. Chem. Soc.*, 2019, **141**, 6310–6317.
61 V. Baltz, A. Manchon, M. Tsoi, T. Moriyama, T. Ono and Y. Tserkovnyak, *Rev. Mod. Phys.*, 2018, **90**, 015005.
62 Y. Nakamura, *J. Magn. Magn. Mater.*, 1983, **31–34**, 829–834.
63 X. G. Zheng, H. Kubozono, H. Yamada, K. Kato, Y. Ishiwata and C. N. Xu, *Nat. Nanotechnol.*, 2008, **3**, 724–726.
64 G. Hausch, *Phys. Status Solidi A*, 1973, **18**, 735–740.
65 S. Khmelevskyi, I. Turek and P. Mohn, *Phys. Rev. Lett.*, 2003, **91**, 037201.